Time-reversal, tori families,\query{Q1} and canards in the Sprott A and NE9 systems

Cite as: Chaos 32, 083119 (2022); https://doi.org/10.1063/5.0097508 Submitted: 29 April 2022 • Accepted: 12 July 2022 • Published Online: 10 August 2022

Taoufik Bakri and D Ferdinand Verhulst







ARTICLES YOU MAY BE INTERESTED IN

Unexpected advantages of exploitation for target searches in complex networks Chaos: An Interdisciplinary Journal of Nonlinear Science 32, 083118 (2022); https:// doi.org/10.1063/5.0089155

A global bifurcation organizing rhythmic activity in a coupled network Chaos: An Interdisciplinary Journal of Nonlinear Science 32, 083116 (2022); https:// doi.org/10.1063/5.0089946

Impact of demographic variability on the disease dynamics for honeybee model Chaos: An Interdisciplinary Journal of Nonlinear Science 32, 083120 (2022); https:// doi.org/10.1063/5.0096638

APL Machine Learning Open, quality research for the networking communities Now Open for Submissions **LEARN MORE**

Time-reversal, tori families, and canards in the **Sprott A and NE9 systems**

Cite as: Chaos **32**, 083119 (2022); doi: 10.1063/5.0097508 Submitted: 29 April 2022 · Accepted: 12 July 2022 ·

Published Online: 10 August 2022







Taoufik Bakria and Ferdinand Verhulst (1)

AFFILIATIONS

Mathematisch Instituut, University of Utrecht, PO Box 80.010, 3508 TA Utrecht, The Netherlands

^{a)}Author to whom correspondence should be addressed: taoufik.bakri@tno.nl.

Also at: TNO Sustainable Urban Mobility & safety, PO Box 96800, 2509 JE The Hague, The Netherlands.

b)Electronic mail: f.verhulst@uu.nl

ABSTRACT

Quadratic three-dimensional autonomous systems may display complex behavior. Studying the systems Sprott A and NE9, we find families of tori and periodic solutions both involving canards. Using time-reversal and symmetry, we are able to explain in these two systems both the analysis and origin of tori, periodic solutions, and the numerics of these objects. For system NE9, unbounded solutions exist that admit analytic description by singular perturbation theory of the flow near infinity, also we observe torus destruction and a new chaotic attractor (Kaplan-Yorke dimension 2.1544) produced by a period-doubling scenario. The subtle numerics of periodic solutions involving canards is explained in the final section.

Published under an exclusive license by AIP Publishing. https://doi.org/10.1063/5.0097508

In dissipative systems, the presence of an infinite family of tori is unusual. We explain these phenomena for two systems of ODEs, Sprott A and NE9, by showing certain symmetries in the systems. A remarkable additional aspect is that the tori show canard behavior. Because of the canards, the presence of periodic solutions on the tori present special numerical integration problems. There are more surprising phenomena in both simplelooking systems: chaotic behavior in both systems and in system NE9 an isolated invariant manifold with in its neighborhood again canard solutions, produced by a stability transition of the manifold.

I. INTRODUCTION

A number of chaotic three-dimensional systems, in fact 17 autonomous systems with linear and quadratic terms only and one parameter (a), have been listed and studied in Ref. 7; see also Ref. 15; all these systems are dissipative, i.e., the three-dimensional phaseflow is not volume-preserving. The systems are numbered NE1, ..., NE17 with one of them, called Sprott A (or NE1). The study of these 17 systems is very instructive as three-dimensional systems generally show much more complexity than two-dimensional ones and as

the 17 systems are relatively simple, quadratic and, with one parameter. The evidence for chaos in Ref. 7 is mainly numerical and an interesting start.

A remarkable aspect of the systems Sprott A and NE9 is the observed presence of families of invariant tori, known in conservative systems, but in contrast, we have here dissipative systems with the parameter small a. This aspect was studied in more detail for Sprott A in Refs. 12 and 13 who correctly observe that we have a kind of KAM (Kolmogorov-Arnold-Moser) tori.

A novel result is that we can complete the theoretical picture both for Sprott A and NE9 by linking the tori bifurcation phenomenon to time-reversal and canards. The scalings near the origin of phase-space in Secs. II and III are related to geometric desingularization of degenerate singularities. For the vast literature, see Refs. 8 and 11. For both systems, we can identify a number of periodic solutions on the tori. For the Sprott A system, unbounded solutions can only be found on the z axis. Another novel aspect is that for system NE9, this is different; we find "rings" of initial values leading to unbounded solutions. Scaling near infinity and using again geometric singular perturbation theory provides insight into this dynamics.

We formulate the equations. The system Sprott A is

$$\dot{x} = y, \ \dot{y} = -x - yz, \ \dot{z} = y^2 - a,$$
 (1)

with $a \ge 0$. The Sprott A system is a special case of the Nosé–Hoover oscillator; for the physics references of this oscillator and a nice introduction to the theory, see Ref. ¹⁴. For a number of a values, the system (1) suggests chaotic behavior; if $a \ne 0$, no equilibria exist. In Ref. 7, the case a = 1, x(0) = 0, y(0) = 5, and z(0) = 0 of system (1) produces a structure that looks like an attractor. The "attracting" object has Kaplan–Yorke dimension 3.0, see Ref. 7.

System NE9 shows related but also different characteristics. The equations are

$$\dot{x} = y, \ \dot{y} = -x - yz, \ \dot{z} = -xz + 7x^2 - a, \ a \ge 0.$$
 (2)

System NE9 has no equilibrium if $a \neq 0$.

A. Setup of the paper

In the Introduction section, we formulate a number of useful lemmas for periodic solutions in the Sprott A and NE9 systems, and we observe the time-reversal character of the two systems. In Sec. II, we consider the Sprott A system adding more details to the canard results of Ref. 1 producing for $0 < a \ll 1$ pulse-like behavior of the solutions. Time-reversal leads to the presence of a tori family around a periodic solution that serves as an organizing center. Infinite families of tori are typical for Hamiltonian systems, see Ref. 2. It is interesting to find such families in dissipative systems. We expect to find periodic solutions on the tori with rather long periods because of their passage through slow manifolds. It takes subtle numerical methods to find the periodic solutions, both stable and unstable (see Sec. V for comments on the numerics). More insight in the presence of tori and the transition to chaos is obtained by using the frequency method of Laskar, see Subsection II D.

A striking difference between the Sprott A and NE9 systems is the presence of families of unbounded solutions in NE9. The behavior near infinity requires again singular perturbation analysis and yields insight into the presence of domains where solutions are attracted to infinity. In system NE9, a chaotic attractor with Kaplan–Yorke dimension 2.1544 is detected that emerges from a period doubling sequence. It is demonstrated how periodic solutions, tori, and chaos are connected.

B. Some useful observations

Consider systems (1) and (2). For arbitrary a, the z axis is an invariant manifold with, if $a \neq 0$, unbounded solutions,

$$sx = y = 0, z(t) = z(0) - at.$$
 (3)

An interesting discrete symmetry feature of (1) is

Lemma I.1. If [x(t), y(t), z(t)] is a solution of system (1) then also [-x(t), -y(t), z(t)] is a solution.

This is verified by substitution. An important feature involving time-reversal of (1) is

Lemma I.2. If [x(t), y(t), z(t)] is a solution of system (1), then by putting $\bar{x} = x, \bar{y} = -y, \bar{z} = -z$ and reversing time $\tau = -t$, $[\bar{x}(\tau), \bar{y}(\tau), \bar{z}(\tau)]$ is also a solution.

Such time-reversal symmetry is called *R*-symmetry in Ref. 9. For system NE9, we have a similar reversibility as in Lemma I.2:

Lemma I.3. If [x(t), y(t), z(t)] is a solution of system (2), then by putting $\bar{x} = -x, \bar{y} = y, \bar{z} = -z$ and reversing time $\tau = -t$, $[\bar{x}(\tau), \bar{y}(\tau), \bar{z}(\tau)]$ is also a solution.

By differentiating the equation for x, we rewrite system (1) as

$$\ddot{x} + \dot{x}z + x = 0, \ \dot{z} = \dot{x}^2 - a.$$
 (4)

Consider the Sprott A system in the form (4). It is easy to prove the following lemma:

Lemma I.4. Assume that $x(t) = \xi(t), y = d\xi/dt, z(t) = \zeta(t)$ are T-periodic (T > 0) solutions of system (4) for a > 0, then

$$\int_0^T \zeta(t)dt = 0. (5)$$

Proof. The equation for *x* with $z = \zeta(t)$ becomes

$$\ddot{x} + \zeta(t)\dot{x} + x = 0.$$

According to the Floquet theory, the solutions of the *x*-equation are of the form $\exp(Bt)\Phi(t)$ with *T*-periodic matrix $\Phi(t)$ and constant 2×2 matrix *B*. For the characteristic exponents λ_1, λ_2 , we have in the periodic case

$$\lambda_1 + \lambda_2 = \frac{1}{T} \int_0^T \zeta(t) dt = 0,$$

which proves the lemma (the corresponding multipliers ρ_1 , ρ_2 satisfy the relation $\rho_1\rho_2=1$).

A different proof adds insight into the periodic solutions of system (1).

Alternative proof of Lemma I.4

Consider for the solutions of system (4) the function

$$F(x, y, z) = \frac{1}{2}(x^2 + y^2 + z^2).$$
 (6)

Differentiation and using the equations yields easily

$$\frac{dF}{dt} = -az,$$

o

$$F(x(t), y(t), z(t)) = F(x(0), y(0), z(0)) - a \int_0^t z(s) ds.$$

If (x.y.z) is T-periodic, we have F(x(0), y(0), z(0)) = F(x(T), y(T), z(T)) and so, if a > 0,

$$\int_0^T z(s)ds = 0.$$

The additional insight is that the quantity F(x(0), y(0), z(0)) is conserved with error O(a) on periodic solutions.

It was observed and proved by averaging in Ref. ! 12 that Sprott A system (1) has a periodic solution near the origin of phase-space and for $0 < a \ll 1$. The scaling needed is $x = \varepsilon \bar{x}, y = \varepsilon \bar{y},$ $z = \varepsilon \bar{z}, a = \varepsilon^2 a_0$ with a_0 being a positive constant. The location is given by $(x(0), y(0), z(0)) = (\sqrt{2a_0}, 0, 0)$. According to Ref. 1, the periodic solution exists also for system NE9 with the same scaling; the location for NE9 is given by $(x(0), y(0), z(0)) = (\sqrt{2a_0/7}, 0, 0)$. In both systems, the periodic solution is neutrally stable to second order approximation.

Using Poincaré compactification, it was shown in Ref. 13 for the Sprott A system that the only orbits that can reach infinity are the solutions starting on the *z* axis. So all solutions starting outside

the *z* axis are bounded. The proof does not carry over to system NE9; it is easy to find solutions escaping to infinity numerically.

II. THE SPROTT A SYSTEM

We summarize the degenerate case a=0 studied in Ref. 12 as the dynamics for $0< a\ll 1$ shows very interesting different aspects. We will use the spherical radius R and the distance r to the z axis defined by

$$R^2 = x^2 + y^2 + z^2, r^2 = x^2 + y^2.$$
 (7)

A. The limit case a = 0

It was shown in Ref. 12 that for a = 0, the behavior is more regular, in fact integrable. We summarize the following:

- If a = 0, x = y = z = 0 is a degenerate critical point of the vector field (equilibrium of the system).
- We differentiate using system (1)

$$\frac{d}{dt}(R^2) = 2(x\dot{x} + y\dot{y} + z\dot{z}) = -2az.$$

So if a = 0, the spheres with radius R are invariant manifolds of the system, but the system (1) is still dissipative.

• If a = 0, the z axis consists of equilibria puncturing the invariant spheres in north- and south-pole. If 0 < R < 2, the south-pole is an unstable focus, the north-pole a stable focus on each invariant sphere. To see this, we differentiate the vector field of system (1),

$$\begin{pmatrix} 0 & 1 & 0 \\ -1 & -z & -y \\ 0 & 2y & 0 \end{pmatrix}.$$

If $(x, y, z) = (0, 0, \pm R)$, the eigenvalues are on the invariant sphere with radius R: $\frac{1}{2}(R \pm \sqrt{R^2 - 4})$ (north-pole) and $\frac{1}{2}(+R \pm \sqrt{R^2 - 4})$ (south-pole). If $R \ge 2$, the two pole equilibria are nodes, for z(0) > 2, respectively, stable and unstable. The implication is that for 0 < z(0) < 2, the solutions near the invariant z axis are winding toward the axis in the x, y plane; for -2 < z(0) < 0, the solutions near the invariant z axis are winding outward in the x, y plane with respect to the z axis.

B. Slow-fast and canard behavior for small a

Consider now the case $a = \varepsilon$ (a small, positive parameter). We choose the initial values of (x,y,z) in an interior subset D of the sphere with R=2. If $x(0)^2+y(0)^2+z(0)^2<4$, we keep the rotating character of the flow around the z axis observed for a=0. It was shown in Ref. 1 that if a is small, we have a singular perturbation problem with canard behavior; the behavior of the solutions for a=0 and $0 < a \ll 1$ is dynamically and topologically very different. We will give the analysis in more detail here, add quantitative aspects, and discuss its geometric consequences.

If *a* is small, it is basic to see system (1) as a slow–fast system and to apply Tikhonov's theorem. ¹⁶ Note that

$$\frac{dr^2}{dt} = -\dot{x}^2 z,$$

so, as long as z(t) is positive, the (x,y) phase-flow is strongly damped, and if z(t) is negative, the flow is excited. When starting with O(1) initial values and z(0)>0, the time needed to produce $x(t),y(t)=O(\sqrt{\varepsilon})$ is $O(|\ln\varepsilon|)$. To put the system in the formulation of Tikhonov's theorem, we rescale: $x=\sqrt{\varepsilon\bar{x}},y=\sqrt{\varepsilon\bar{y}}$. Omitting the bars, system (1) becomes

$$\dot{x} = y, \ \dot{y} = -x - yz, \ \dot{z} = \varepsilon(y^2 - 1),$$
 (8)

and rescaling time $\tau = \varepsilon t$, we find the equivalent system

$$\varepsilon \frac{dx}{d\tau} = y, \ \varepsilon \frac{dy}{d\tau} = -x - yz, \ \frac{dz}{d\tau} = y^2 - 1. \tag{9}$$

According to the geometric singular perturbation theory system, (8) shows fast motion of the x,y-component except in an $O(\varepsilon)$ neighborhood of the one-dimensional slow (or critical) manifold, M_0 defined by

$$y = 0, -x - yz = 0. (10)$$

The slow manifold M_0 corresponds with the z axis in three-dimensional phase-space; it is normally hyperbolic when excluding a neighborhood of z=0 as we have for the fast part of the system that the real part of the spectrum is -z/2. M_0 approximates the smooth slow manifold M_ε that exists for solutions of system (8). According to section 15.7 of Ref. 18, when excluding a neighborhood of z=0, M_0 approximates M_ε exponentially close. To fix ideas, we take initially

$$x(0) = x_0, y(0) = 0, z(0) = z_0, 0 < x_0, z_0 < 2.$$

We assume that x_0, z_0 are not ε -close to 0 or 2. According to Tikhonov, we have when starting outside M_0 at positive $z(0) = z_0$ an $O(\varepsilon)$ approximation of the fast solutions of system (8) of the form

$$X_0(t) = x_0 e^{-z_0 t/2} \cos\left(\sqrt{4 - z_0^2} \, \frac{t}{2}\right). \tag{11}$$

The approximation is valid on an interval O(1) in τ , $O(1/\varepsilon)$ in t as long as we do not enter a ε -neighborhood of M_0 . From (11), we can estimate the fast time T_1 needed to approach M_0 ,

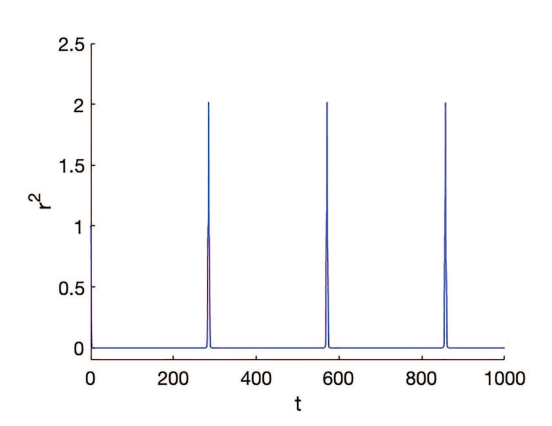
$$x_0 e^{-z_0 T_1/2} \cos\left(\sqrt{4 - z_0^2} \frac{T_1}{2}\right) = \varepsilon.$$
 (12)

Ignoring the oscillations, a rough estimate is

$$T_1 \le -\frac{2}{z_0} \ln \left(\frac{\varepsilon}{x_0} \right).$$
 (13)

The approximate time needed for the motion until z=0 along M_0 is $T_2=z_0/\varepsilon$. Using the symmetry result of Lemma I.2, we find the estimate of the return time $T\geq 2(T_1+T_2)$ of the flow in system (8). The pulse-like behavior for the fast motion of the flow is shown in Fig. 1. The slow-fast system (8) is actually valid in an $O(\sqrt{\varepsilon})$ neighborhood of the origin, whereas in Fig. 1, we start the solutions outside this region; this is possible because of the strong damping if z(t)>0, but it will produce a lower bound of the return time.

Geometric singular perturbation theory in combination with time-reversal and symmetry produces the behavior shown in the Poincaré maps of Fig. 2. Increasing ε , we expect the tori to break up, perhaps with Cantor gaps as in near-integrable Hamiltonian systems.



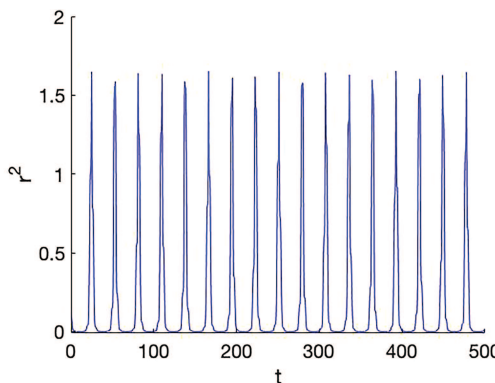


FIG. 1. Pulses of $r^2(t)$ showing the fast motion of the (x, y)-flow with respect to the z axis that is near the slow manifold. In the left, we have a = 0.01, x(0) = 1, y(0) = 0, z(0) = 1, and in the right, a = 0.1, x(0) = 0.3162, y(0) = 0, z(0) = 1. The behavior near the z axis shows canard behavior.

C. Tori and periodic solutions for small a

In this subsection, periodic orbits will be described obtained by the procedure outlined in Sec. V.

It has become clear that Lemma I.2 regarding time-reversal and symmetry plays an essential part in producing recurrence of the canards and tori-like structures. As we will show in Subsection II E, unfolding system (1) destroys the reversal symmetry and the tori-like structures. Time-reversal symmetry plays a part in what is sometimes called "dissipative KAM theory," see for surveys Refs. 3, 9, and 14.

For the Sprott A system this, was conjectured in 12 and 13 with strong numerical evidence. There exist a large number of papers describing the emergence of quasi-periodic solutions and tori near equilibria with purely imaginary eigenvalues, sometimes in three-space with a zero eigenvalue added. However, the framework for the Sprott A system is different as for a (or ε) zero, we have an infinite set of equilibria, whereas for a > 0, we have no equilibrium in the

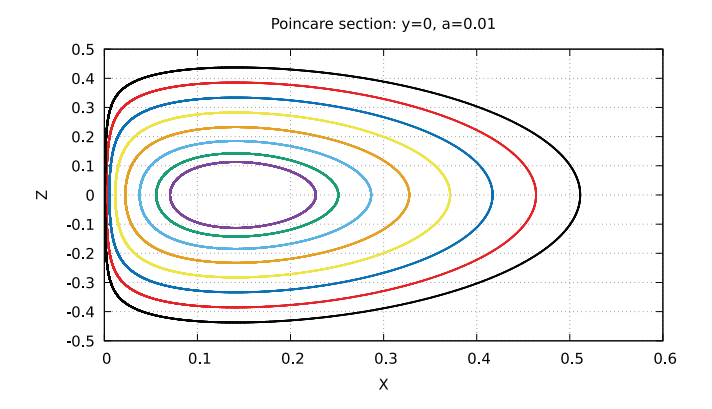


FIG. 2. Poincaré maps in the plane y=0 of the Sprott A system (1) near the origin of phase-space for a=0.01. The behavior near the z axis shows canard behavior for various initial conditions.

system, and the infinite set persists as invariant manifold of the system. For a=0, phase-space is foliated into invariant spheres that collapse to tori for $0 < a \ll 1$. In our analysis, we have a periodic solution at $O(\varepsilon)$ distance of three-dimensional phase-space. This periodic solution is surrounded by the infinite set of slow–fast solutions we derived in Subsection. II B. This follows from the estimates in section 15.7 of Ref. 18 when excluding a neighborhood of z=0 and the time-reversal characteristic.

It makes sense to have a closer look at the tori. First, we note that the theory of canards guarantees the presence of slow manifolds for a small enough. The slow manifolds are tunneling exponentially close to the z axis parametrized by z(0). The reversibility result of Lemma I.2 yields a tori family of which the dynamics still has to be explored.

It is interesting to look for periodic solutions embedded in tori by using Lemma I.4. Define

$$I(t) = \int_0^t z(s)ds.$$

Look for T-periodic zeros of I(t), maybe varying ε for fixed z_0 ; T will be close to the return times of the tori.

It might help us to consider maps of the x, I-plane into itself for y = 0. These maps will be used to find periodic solutions numerically later on.

It was shown in Refs. 12 and 13 and to the second order in Ref. 1 that on scaling $x, y, z = O(\varepsilon)$ and $a = \varepsilon^2 a_0$, a Lyapunov stable periodic solution exists $O(\varepsilon^2)$ -close to the invariant manifold z = 0 and the circle $x^2 + y^2 = 2a_0\varepsilon^2$. As a_0 is an arbitrary O(1) constant, this means that we have found a family of periodic solutions that gives for each fixed a an *organizing center* of the family of tori. See Fig. 3. An example of this family is periodic orbit 2 of Table I.

A different periodic solution is shown in Fig. 4. This periodic solution of system (1) in a torus near the origin is found by numerical bifurcation analysis for a = 0.013149; x(0) = -0.0985, y(0) = 0.09811, andz(0) = 0.9951. The slow manifold shows up in the center of the (x, y) projection (left figure) and in the vertical z motion in the (x, z) projection (middle); the observed asymmetry in the (x, y) projection gives us the mirrored periodic solution (right in

figure) guaranteed by Lemma I.1. For the three Lyapunov exponents of this periodic solution, we find zero.

Numerical integrations show that the recurrence of the orbits in the tori is generally not periodic, but we can find more isolated, stable periodic solutions; see again Table I. We have strong dependence of the tori on the initial conditions $[x(0), y(0)) = O(\sqrt{\varepsilon}]$ and z(0).

1. The periodic orbits of table I

The Poincaré maps of the periodic orbits show collections of segments that consist of isolated points that correspond with the transitions of the transversal plane of section. Segments arise because of the slow–fast dynamics of the orbits if *a* is small.

The exception is orbit 2 that is part of the family that forms the organizing center of the tori. For orbit 2 in this family, the Poincaré section is a fixed point, and the (x, y) projection is close to a circle.

As mentioned in the caption of Table I, at least seven additional periodic orbits exist because of symmetry considerations. In Fig. 5, we present a few typical examples of Table I. Orbit 8 looks rather complex; we illustrate its behavior with time in Fig. 6 for

x(t), z(t). In accordance with Lemma 5, we find for the z, I-diagram $(I = \int_0^t z(s)ds)$ a closed loop (picture not shown).

The stability of the periodic solutions follows from the 3 Lyapunov multipliers. As the Sprott A system is autonomous, one multiplier ρ_1 will always be 1; Lemma I.4 and the time reversality yield that for the two remaining multipliers, we have $\rho_2 = 1/\rho_3$; see Table II. We have stability if $|\rho_i| = 1$, i = 1, 2, 3.

It is more difficult to find unstable periodic orbits. We list five unstable cases in Table III. The Poincaré sections and projections on the (x, y) plane are shown in Fig. 7

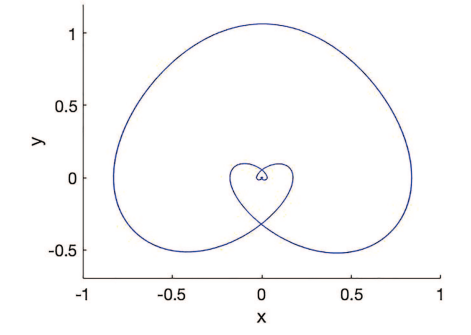
The R-symmetric orbits of Table I have all their complex multipliers on the unit circle; the orbits are Lyapunov stable. It is important to note that there exist also periodic orbits with real multipliers outside the unit circle in the complex plane, they are unstable; see Tables III and IV.

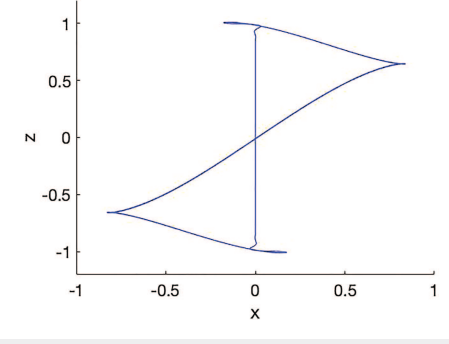
D. Fundamental frequencies in the chaotic regions

The method of fundamental frequencies was first introduced by Laskar in 1990 where he used it to estimate the size of the chaotic zones in a 15 degrees of freedom dynamical system. The idea behind it is that the frequency map is still exactly defined on the Cantor set

TABLE I. Initial values of 11 periodic orbits with a = 0.1. According to Lemma I.1, the seven asymmetric orbits (asymm) yield additional periodic orbits by the symmetry -x(t), -y(t), z(t). In the cases of orbits 1, 2, 8, and 9 with "symm?" in the last column, the orbits are looking symmetric in the (x, y) projection but a proof is lacking.

Orbit	x(0)	y(0)	z(0)	Comment
1	1.869 599 405 933 272 8	0.294 452 058 991 819 9	0.011 086 661 220 298 6	symm?
2	0.429 103 720 566 849 1	0.098 722 569 075 084 1	0.021 838 833 127 457 4	symm?
3	0.474 435 715 195 752 1	0.098 342 667 345 030 0	0.857 675 021 281 200 9	asymm
4	0.277 489 384 298 501 0	0.099 574 978 195 378 2	-1.3419264311707517	asymm
5	2.354 073 257 472 744 1	0.093 024 366 364 032 1	0.003 835 439 436 810 8	asymm
6	1.790 893 256 744 474 4	0.001 415 500 825 757 7	0.0000790590874794	asymm
7	1.343 783 088 166 542 7	-0.0049654722303571	-0.0003694822052058	asymm
8	1.225 723 045 768 512 4	-0.0079551776672382	-0.0006488696242273	symm ?
9	1.467 128 202 691 749 2	-0.0004444199767620	-0.0000302875267243	symm ?
10	2.233 390 196 654 015 3	-0.0066173642003448	-0.0002962481436574	asymm
11	1.742 820 349 983 936 3	-0.0051638432948303	-0.0002962650562144	asymm





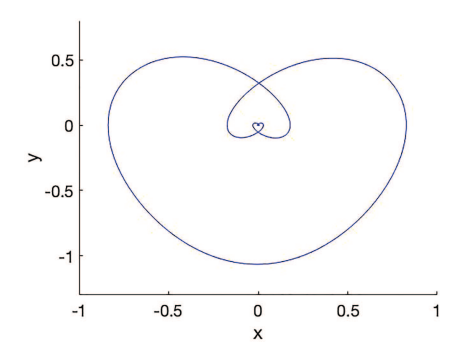


FIG. 4. Periodic solution of system (1) in a torus near the origin of phase-space for a = 0.013149; x(0) = -0.0985, y(0) = 0.09811, z(0) = 0.9951. The vertical motion in the x, z projection (middle) corresponds with the slow manifold. Right: the corresponding mirrored periodic solution with a = 0.013149; x(0) = 0.0985, y(0) = -0.09811, z(0) = 0.9951.

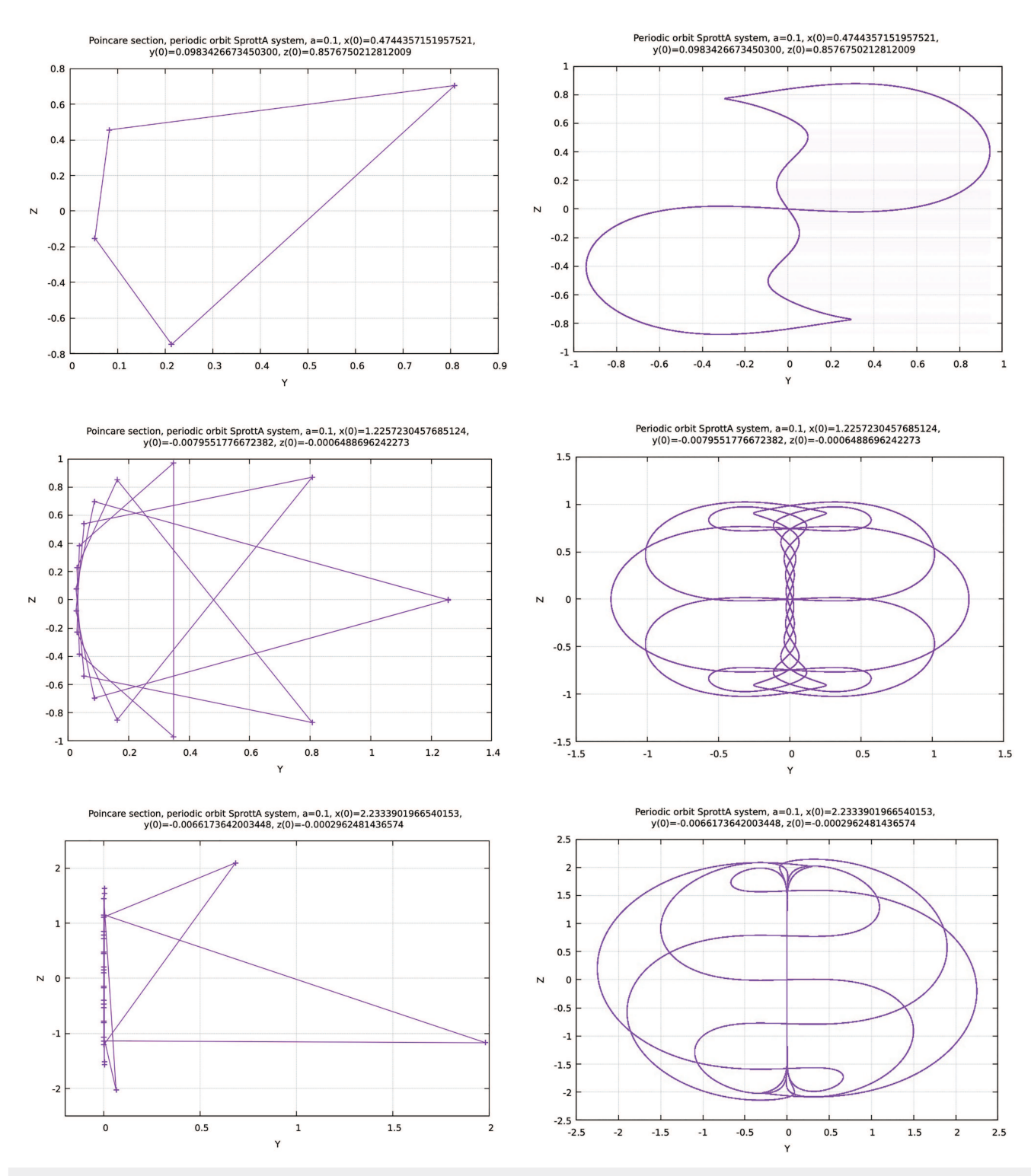
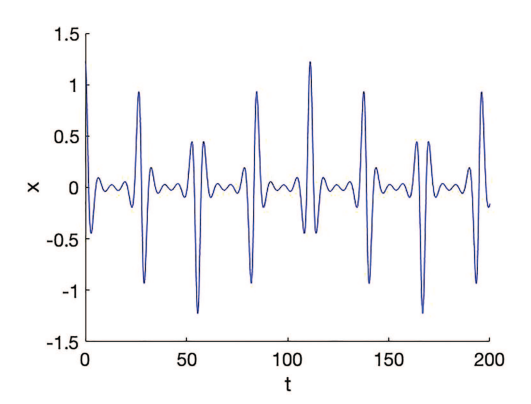


FIG. 5. Periodic solutions of system (1) from Table I. Successive orbits 3 (asymmetric but simple), 8, and 10 (more complex orbits). Left are the Poincaré sections consisting of many points; right are the projections on the (x, y) plane.



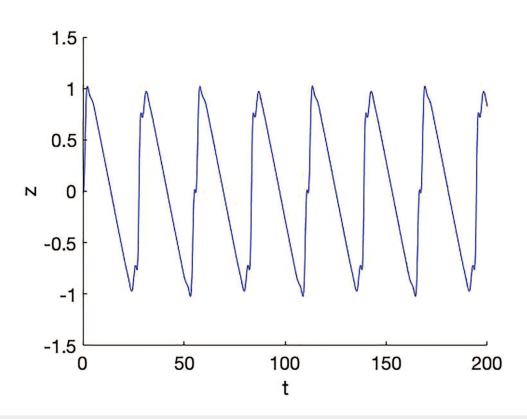


FIG. 6. Timeseries x(t) and z(t) on orbit 8 in Table I.

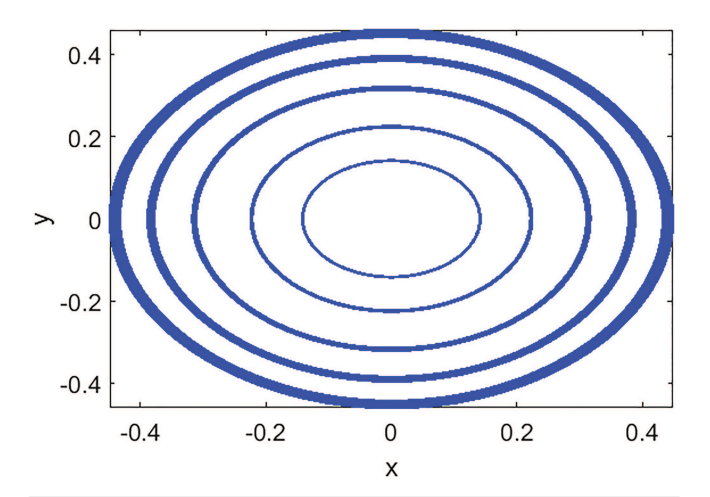


FIG. 3. Five orbits in tori and $O(\varepsilon^2)$ -close to five members of the family of periodic solutions in the Sprott A system (1) with projection in the (x,y) plane given by $x^2 + y^2 = 2a$. We took successively a = 0.1, 0.075, 0.05, 0.025, 0.01 corresponding to y(0) = 0, z(0) = 0.005 75, 0.003, 0.0018, 0.0009, and 0.000 01.

of the invariant tori. It can be thought of as a diffeomorphism on this set. Chaotic zones will, therefore, appear as loss of regularity regions for the frequency map. This approach is more accurate than using Lyapunov exponents and computing the Kaplan–Yorke dimension as the frequency variations directly signal the breakup of invariant tori. This criterion is used here to identify chaotic behavior in the Sprott A system. The fundamental frequencies were computed using the SDDS numerical analysis of the frequencies (NAFF) algorithm by Laskar, see Ref. 10 for more details on the approach of numerical analysis of the frequencies (NAFF).

In Fig. 8, we show the fundamental frequencies as a function of x(0) in the tori and chaotic regions for a = 0.1. Left in Fig. 8, we run x(0) from 0 to 0.13 showing a clear and regular pattern. Right in the figure, we have zoomed in near the origin [-0.0004 < x(0)]

< +0.0004]; near x(0) = 0, we have an accumulation of frequencies and loss of regularity of the frequency map yielding, therefore, chaotic motion in the Sprott A system at parameter value a = 0.1.

E. Unfolding near eigenvalue zero

The time-reversality is essential for our results; we show this by unfolding of the singularity and breaking time-reversality. If a=0, we have a zero eigenvalue for the critical point at the origin. We propose the following unfolding using positive parameter c,

$$\dot{x} = y, \ \dot{y} = -x - yz, \ \dot{z} = y^2 - a - cz.$$
 (14)

Lemma I.2 does not hold anymore, the time symmetry is broken. The z axis is still an invariant manifold; starting at $(x, y, z) = (0, 0, z_0)$, the solution is

$$z(t) = -\frac{a}{c} + \left(z_0 + \frac{a}{c}\right)e^{-ct}.$$
 (15)

If a = 0, c > 0, the origin is a stable focus with one negative eigenvalue and two purely imaginary ones. The spheres $R^2 = x^2 + y^2 + z^2 = \text{constant}$ are no longer invariant manifolds; $dR^2/dt = -2cz^2$.

TABLE II. Periods and multipliers of 11 stable periodic orbits of Table | [system (1)]. Of the 16 decimals, we show for the periods two decimals for the multipliers 4. In each case, $|\rho_i| = 1$, i = 1, 2, 3.

Orbit	Period	Multipliers ρ_1, ρ_2, ρ_3
1	80.35	1; 0.0576 + 0.99839i; 0.0576 - 0.9983i
2	6.21	1; $-0.3702 + 0.9289i$; $-0.3702 - 0.9289i$
3	25.80	1; $0.9822 + 0.1878i$; $0.9822 - 0.1878i$
4	34.40	1; $0.8610 + 0.5086i$; $0.8610 - 0.5086i$
5	98.53	1; $0.5801 + 0.8145i$; $0.5801 - 0.8145i$
6	1.15	1; 0.9878 + 0.1560i; 0.9878 - 0.1560i
7	59.69	1; $0.7648 + 0.6443i$; $0.7648 - 0.6443i$;
8	111.19	1; $0.9952 + 0.0974i$; $0.9952 - 0.0974i$
9	128.46	1; $0.9713 + 0.2379i$; $0.9713 - 0.2379i$
11	149.48	1; $0.9158 + 0.401i$; $0.9158 - 0.401i$

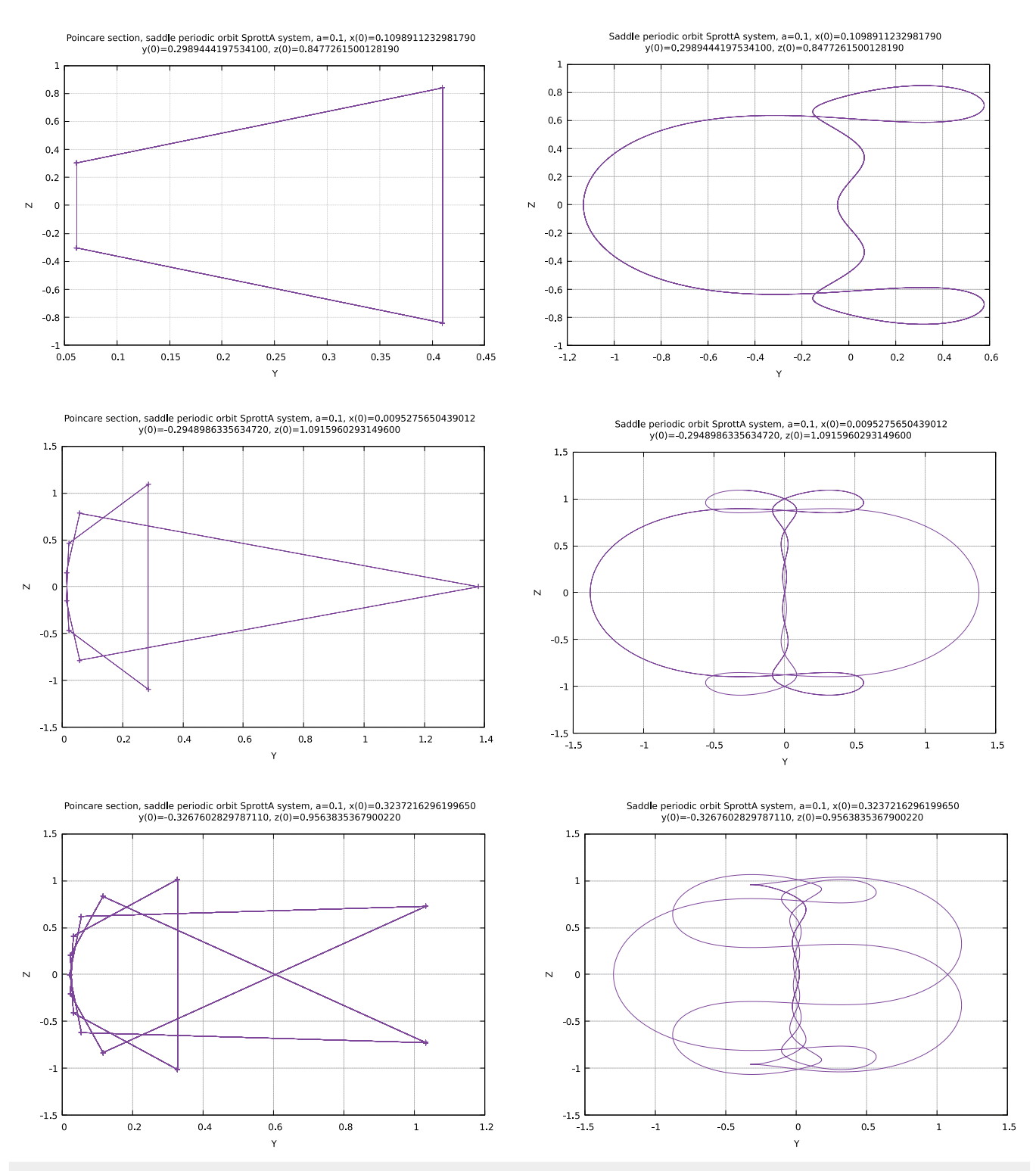
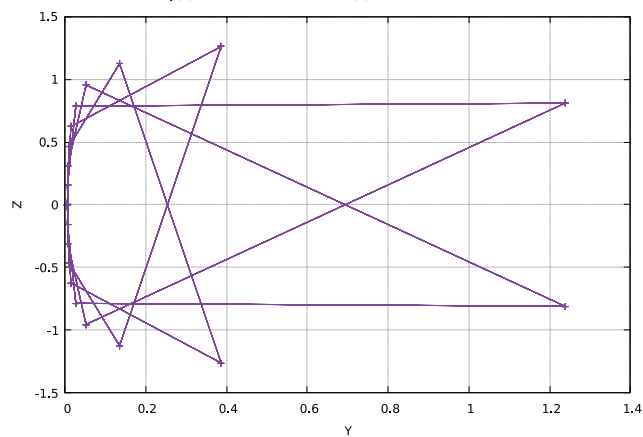
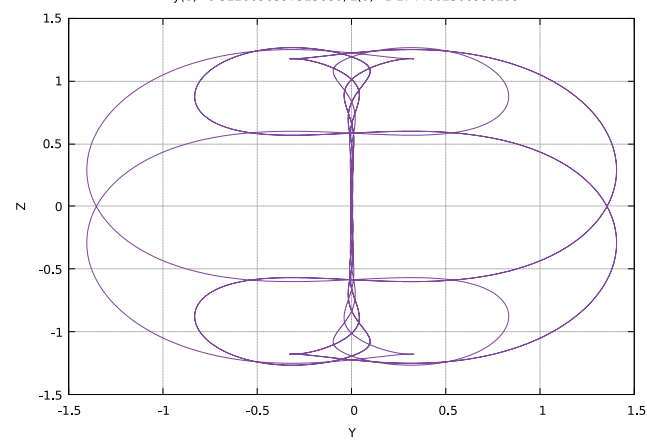


FIG. 7. Five unstable periodic solutions of system (1) from Table III. Left are the Poincaré sections consisting of many points; right are the projections on the (x, y) plane.

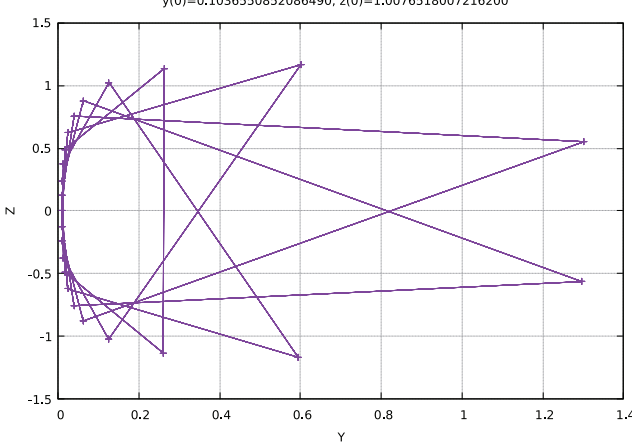
Poincare section, saddle periodic orbit SprottA system, a=0.1, x(0)=-0.4511487807561070 y(0)=0.3220096397325680, z(0)=1.1744662306990299



Saddle periodic orbit SprottA system, a=0.1, x(0)=-0.4511487807561070 y(0)=0.3220096397325680, z(0)=1.1744662306990299



Poincare section, saddle periodic orbit SprottA system, a=0.1, x(0)=0.0205762776384968 y(0)=0.1036550852086490, z(0)=1.0076518007216200



Saddle periodic orbit SprottA system, a=0.1, x(0)=0.0205762776384968 y(0)=0.1036550852086490, z(0)=1.0076518007216200

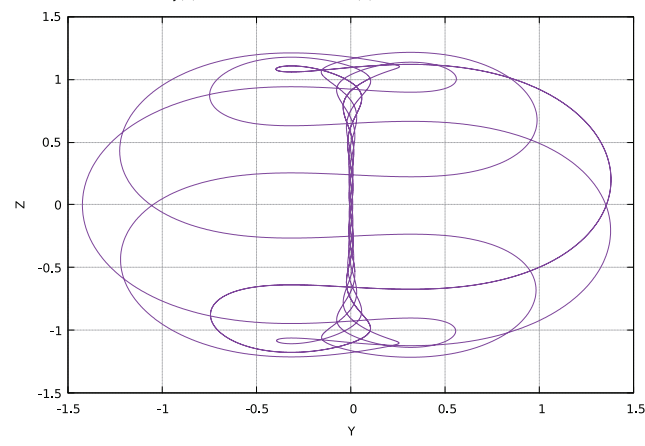


FIG. 7. continued

If a > 0, c > 0, we have on the negative z axis the critical point (x, y, z) = (0, 0, -a/c); if a is fixed and c tends to zero, this critical point moves to minus infinity and is stable. We will characterize the dynamics near the invariant z axis in the case $0 < a, c \ll 1$.

In Eq. (14), we rescale $x = \sqrt{\varepsilon}\bar{x}$, $y = \sqrt{\varepsilon}\bar{y}$, $a = \varepsilon a_0$, $c = \varepsilon c_0$; omitting the bars, we obtain

$$\dot{x} = y, \ \dot{y} = -x - yz, \ \dot{z} = \varepsilon y^2 - \varepsilon a_0 - \varepsilon c_0 z.$$
 (16)

This is a slow–fast system with again slow manifold x = y = 0; the slow manifold is hyperbolic unless z = 0. If z(0) > 0, the (x, y) oscillations are strongly damped and the phase-flow moves to the z axis. The Tikhonov theorem¹⁶ can be used as in the case c = 0. We find again recurrent canard behavior but not the presence of invariant tori as it turns out that the solutions tend for $0 < a, c \ll 1$ to a stable periodic solution near the origin. We show this using a different scaling of Eq. (14): $x = \varepsilon \bar{x}, y = \varepsilon \bar{y}, z = \varepsilon \bar{z}, a = \varepsilon^2 a_0, c = \varepsilon c_0$; omitting

the bars, we obtain

$$\dot{x} = y, \ \dot{y} = -x - \varepsilon yz, \ \dot{z} = \varepsilon y^2 - \varepsilon a_0 - \varepsilon c_0 z.$$
 (17)

Using transformation to cylindrical coordinates,

$$x = r\cos(t + \psi), y = \dot{x} = -r\sin(t + \psi), z = z,$$
 (18)

we find the variational system

$$\begin{cases} \dot{r} = -\varepsilon r \sin^2(t + \psi)z, \\ \dot{\psi} = -\frac{1}{2}\varepsilon \sin(2t + 2\psi)z, \\ \dot{z} = \varepsilon r^2 \sin^2(t + \psi) - \varepsilon(a_0 - c_0 z). \end{cases}$$
(19)

Averaging to first order produces equations governing the approximations for r, ψ, z ,

$$\dot{r} = -\frac{\varepsilon}{2}rz, \ \dot{\psi} = 0, \ \dot{z} = \frac{\varepsilon}{2}(r^2 - 2a_0 - 2c_0z).$$
 (20)

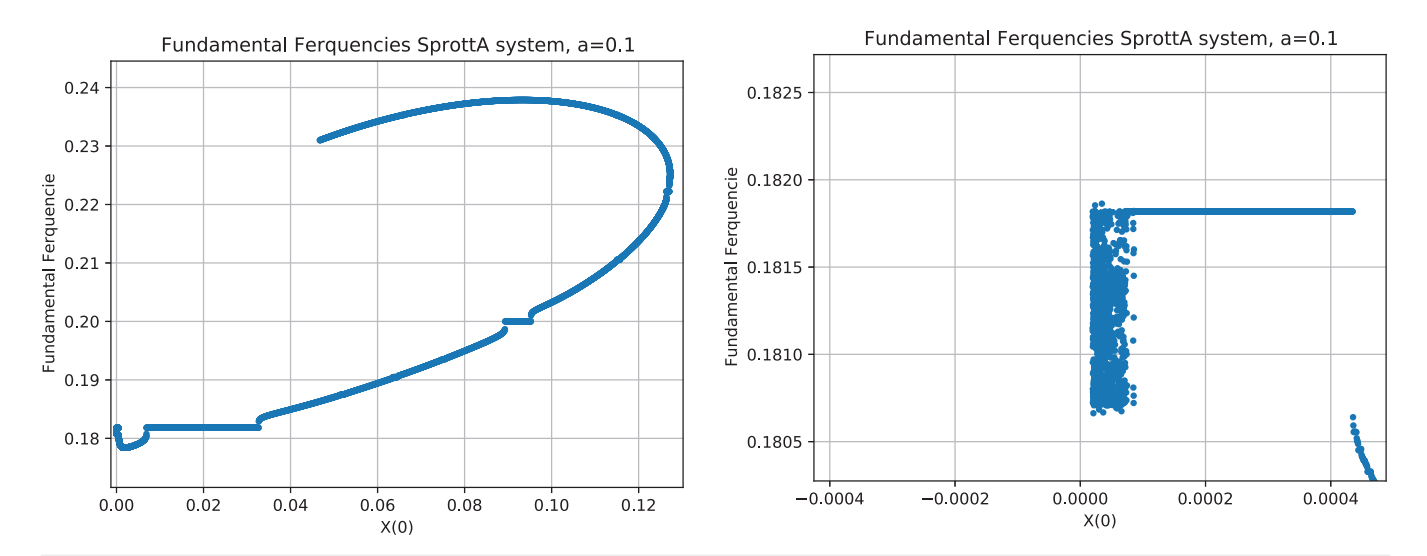


FIG. 8. The frequencies in the neighborhood of the origin in the tori and in the regions between them.

If $r=\sqrt{(2a_0)}$, z=0, we have an equilibrium of the averaged system (20). According to theorem 11.5 in Ref. 17 (the so-called second Bogoliubov theorem), the autonomous system (17) has a periodic solution in an $O(\varepsilon)$ neighborhood of the equilibrium if the $n\times n$ Jacobian matrix at this point has rank n-1; this is the case here. We find two complex eigenvalues and one negative eigenvalue $O(\varepsilon)$, so an isolated stable periodic solution exists in an $O(\varepsilon)$ neighborhood of the origin. The behavior of the Sprott A system unfolded near the origin is similar to the behavior of system NE8, see for details Ref. 1.

III. SYSTEM NE9 FOR PARAMETER a SMALL

The analysis of Sprott A system (NE1) for small *a* carries partly over to system NE9 as similar time-reversal plays a part but there are interesting new aspects like the presence of sets of unbounded solutions, tori destruction, and a new chaotic set.

If a=0, the origin of phase-space is an equilibrium with eigenvalues $\pm i$, 0. The first two equations of system (2) are the same as for the Sprott A system, the implication is that also in system NE9, the (x, y) flow is strongly damped as long as z(t) > 0. See Fig. 9 for the tori that emerge near the origin of phase-space and small a; this region near the origin is smaller than in the case of the Sprott A system.

The behavior of the canards and the corresponding pulses are quantitatively different from the Sprott A system, see Fig. 10

A. Tori and periodic solutions for small a

As in Subsection II C, the numerical analysis of periodic solutions in system NE9 refers to Sec. $\rm V.$

We rescale $x, y, z = O(\varepsilon)$ and $a = \varepsilon^2 a_0$. It was shown in Ref. 1 that a Lyapunov stable periodic solution exists $O(\varepsilon^2)$ -close to the invariant manifold z = 0 and the circle $x^2 + y^2 = \frac{2}{7}a_0\varepsilon^2$. As a_0 is an arbitrary O(1) constant, this means that we have found again a family of periodic solutions that we expect to produce for fixed

a an organizing center of a family of tori. See Fig. 11. Lemma I.3 guarantees time-reversal and symmetry.

To analyze the canards, we use a different scaling. Again, we put $a = \varepsilon$ with small parameter $\varepsilon \ge 0$. As in Sec. II, we put the system in the formulation of Tikhonov's theorem, here by rescaling $x = \varepsilon \bar{x}, y = \varepsilon \bar{y}$. Omitting the bars, system (2) becomes

$$\dot{x} = y, \ \dot{y} = -x - yz, \ \dot{z} = \varepsilon(-xz + 7\varepsilon x^2 - 1).$$
 (21)

The slow manifold M_0 corresponds as before with the z axis in three-dimensional phase-space; it is normally hyperbolic when excluding a neighborhood of z=0. M_0 approximates the smooth slow manifold M_ε that exists for solutions of system (21) exponentially close when excluding a neighborhood of z=0 (see again section 15.7 of Ref. 18). As for system NE1, the family of canard solutions surround the small family of periodic solutions near the origin as in Subsection I B.

From the canard behavior, we have via time-reversal and symmetry (Lemma I.3) the emergence of tori for parameter small a. However, the pulses for system NE9 in Fig. 10 show more variation than in the NE1 case. These variations are caused by the different terms in the z-equation.

In Fig. 12, we show a few examples of periodic solutions.

IV. SYSTEM NE9, BOUNDEDNESS AND CHAOS

System NE9 has many other interesting features if we admit larger values of the parameter a. We will discuss boundednes of solutions and explore for O(1) values of parameter a the presence of tori and strange attractors.

A. Bounded and unbounded solutions

Consider again system NE9 (2) but now regarding boundedness of the solutions. In Fig. 13, we present regions of initial conditions (yellow) that produce unbounded solutions if a = 0.01; the

black regions correspond with initial conditions for bounded solutions. We repeat the search for bounded and unbounded solutions for a-=0.55, see the results in Fig. 14.

The numerics shows that z(t) becomes unbounded; y(t) tends in this case to zero, whereas x(t) tends to a fixed number, dependent on the initial conditions, see Fig. 13. Using this information, we give arguments for the behavior near infinity by transforming z = 1/w; system (2) becomes

$$\dot{x} = y, \, \dot{y} = -x - \frac{y}{w}, \, \dot{w} = xw - 7x^2w^2 + aw^2, \, a \ge 0.$$
 (22)

We have that w=0 is a solution if y(t) tends to zero and faster than w(t); another condition will be that for certain t_0 and $t \ge t_0$, we have x(t) < 0. Suppose that $w(t) \ne 0$ but $O(\varepsilon)$. We rescale $w = \varepsilon \bar{w}$, system (22) can be written as

$$\dot{x} = y, \ \varepsilon \dot{y} = -\varepsilon x - \frac{y}{\bar{w}}, \ \dot{\bar{w}} = x\bar{w} - \varepsilon 7x^2\bar{w}^2 + \varepsilon a\bar{w}^2, \ a \ge 0.$$
 (23)

According to singular perturbation theory, see Ref. 18, y(t), $t \ge t_0$ moves to zero in a fast fiber if $w(t_0) > 0$ with timelike variable t/ε , \bar{w} tends to zero with timelike variable t. This shows that w = 0, with the assumptions given above, corresponds with a set of solutions of system (22); we have for this set $y(t) \to 0$ and x(t) tends to $x_c = x(t_0) + O(\varepsilon)$. The computation gives also a hint regarding the origin of the structure of "rings" of initial conditions leading to bounded and unbounded solutions. We noted that for w = (1/z) = 0 to be an attractor, we have the condition x(t) < 0, $t \ge t_0$. We expect that for various starting values of x(t), this component of the system will still oscillate before it enters the neighborhood of w = 0 for $t \ge t_0$. Its sign at $t = t_0$ will determine the final boundedness.

As qualitative arguments, this reasoning is sound but note that the analysis of the quantitative behavior is for a large part numerical.

TABLE IV. Periods and multipliers of five unstable periodic orbits of Table III [system (1)]. Of the 16 decimals, we show for the periods two decimals for the multipliers 4.

Orbit	Period	Multipliers ρ_1 , ρ_2 , ρ_3
1B	25.82	1; 0.8278; 1.2080
2B	59.85	1; 0.4951; 2.01977
3B	85.44	1; 0.9858; 1.0144
4B	128.46	1; 0.7867; 1.2711
5B	307.59	1; 0.9779 1.0226

1. The case a = 1

A special unbounded solution arises if a = 1. We find on the manifold z = 7x the solutions

$$x(t) = -\frac{t}{7} + x(0), y = -\frac{1}{7}, z(t) = -t + 7x(0).$$
 (24)

The family of solutions is parameterized by x(0); the sign of x(0) is for a=1 clearly not important. Linearization of system (2) for a=1 at this special solution produces structural stability of the solution when a neighborhood of x=0 is excluded. The solution is asymptotically stable if x>0 and unstable if x<0. The structural stability implies continuation for a finite interval of time when excluding a neighborhood of x=0. This agrees with the picture of Fig. 16 where a=0.99. The solution for a=0.99 follows the set z=7x and shows canard behavior when passing the region where x=0. We transform $x, y, z \mapsto x, v, w$ by

$$x = x, y = y, w = z - 7x.$$
 (25)

We find the system satisfying w = 0, a = 1,

$$\dot{x} = y, \ \dot{y} = -x - yw - 7xy, \ \dot{w} = -xw - 7y - a.$$
 (26)

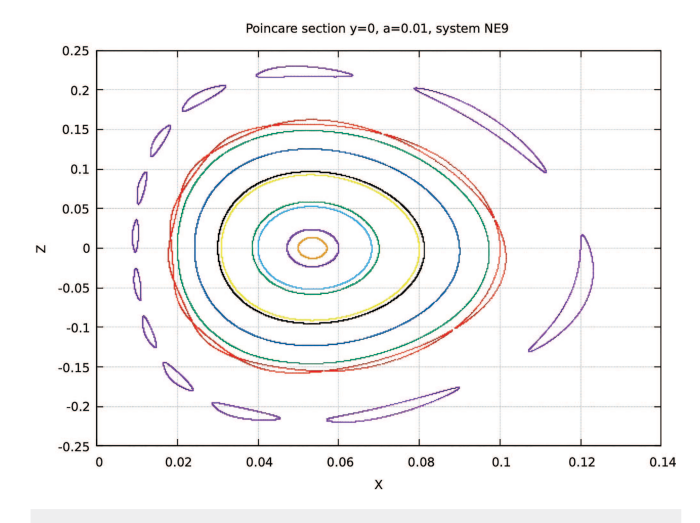
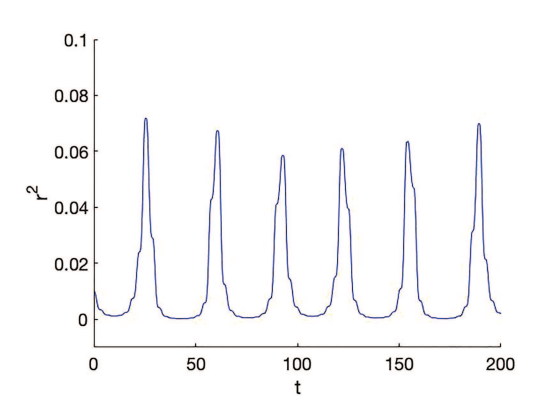


FIG. 9. Poincaré map in the plane y=0 of system (2) near the origin of phase-space for a=0.01. The numerics shows tori near the origin of phase-space as in the Sprott A system.

TABLE III. Initial values of five periodic orbits with a = 0.1. According to Lemma I.1, the three asymmetric orbits (asymm) correspond with a periodic orbit -x(t), -y(t), z(t). In the cases of orbits 2B,4B, the orbits are looking symmetric in the x, y projection but a proof is lacking.

Orbit	x(0)	y(0)	z(0)	Comment
1B	0.109 891 123 298 179 0	0.298 944 419 753 410 0	0.847 726 150 012 819 0	asymm
2B	0.009 527 565 043 901 2	-0.2948986335634720	1.091 596 029 314 960 0	symm?
3B	0.323 721 629 619 965 0	-0.3267602829787110	0.956 383 536 790 022 0	asymm
4B	-0.4511487807561070	0.322 009 639 732 568 0	1.174 466 230 699 029 9	symm?
5B	0.020 576 277 638 496 8	0.1036550852086490	1.0076518007216200	asymm



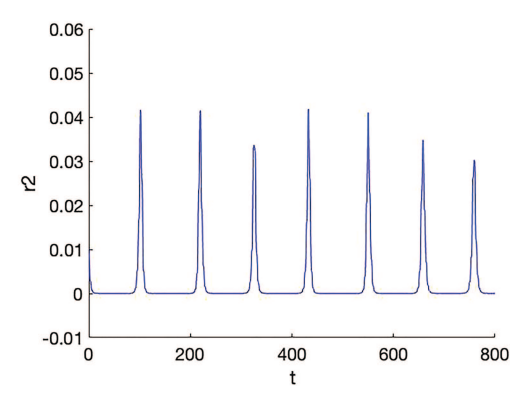


FIG. 10. Pulses of $r^2(t)$ showing the fast motion of the (x, y)-flow with respect to time including the slow manifold for system (2), NE9. Left we have a = 0.05, x(0) = 0.1, y(0) = 0, and z(0) = 0.4; right the same initial conditions but a = 0.01. The behavior near the z axis shows canard behavior, but for a = 0.01, the pulses are more irregular.

In Fig. 15, the bounded solutions are shown in yellow regions of the x, z-diagram for a=1 and a=0.99. Choosing a close to 1, say, $a=1-\varepsilon$, the structural stability of the exact solution enables us to approximate w(t) as long as we do not enter a neighborhood of x=0. We have no need for the usual slow manifold scaling. We find with exact solution (24) for the equation with approximate w(t),

$$\dot{w} = -(x(0) - \frac{t}{7})w + \varepsilon, w(0) = 0.$$
 (27)

The approximate solution is

$$w(t) = \varepsilon e^{(-x(0)t + \frac{t^2}{14})} \int_0^t e^{(x(0)s - \frac{s^2}{14})} ds, \ 0 \le t \le 7x(0).$$

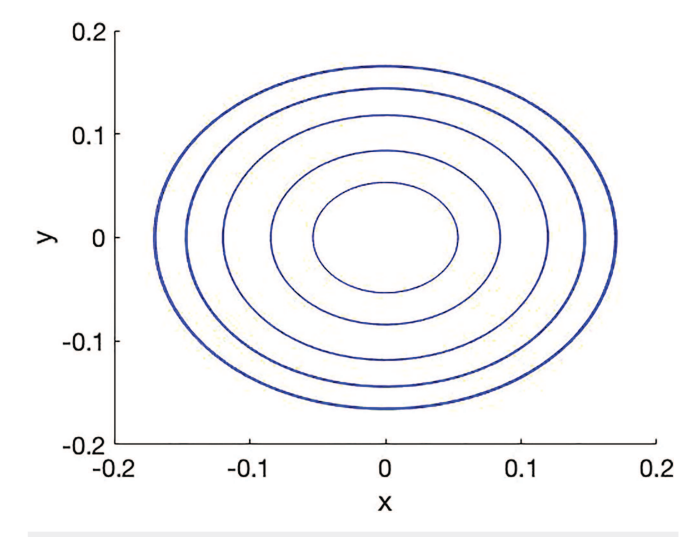


FIG. 11. Five orbits in tori and $O(\varepsilon^2)$ -close to five members of the family of periodic solutions in the NE9 system (2) with projection in the (x,y) plane given by $x^2+y^2=\frac{7}{2}a$. We took successively a=0.1,0.075,0.05,0.025, and 0.01.

The term $t^2/14$ dominates the expression with consequence that the canard behavior, following the manifold z=7x where it has become unstable, depends with $O(\varepsilon)$ on x(0). This is confirmed by the numerics of the system, see Fig. 16. We find a family of periodic solutions with canard behavior as the slow manifold z=7x is followed for some time where it is unstable, but as $w(7x(0)) = O(\varepsilon)$, the solutions are very close (in Fig. 16 $\varepsilon = 1 - a = 0.01$).

2. Bifurcation analysis of the periodic orbit near the canard

Continuation of the periodic orbit at a = 0.99 with respect to the parameter a yields the following bifurcation diagram. See Fig. 17.

Continuation of the periodic solution with respect to the parameter a and starting at a=0.99 yields twice a period doubling. The first one occurs at $a=5.753\,79\times10^{-1}$ where the orbit undergoes a supercritical period-doubling bifurcation with normal form coefficient $l_1=-4.893\,206\times10^{-5}$ and period T=8.24 becomes unstable and a stable period 2 orbit bifurcates from it. The unstable periodic period 1 orbit undergoes a second supercritical period-doubling bifurcation with normal form coefficient $l_1-6.610\,245\times10^{-3}$ and period T=6.93 at the parameter value $T=6.610\,245\times10^{-3}$ and period T=6.93 at the parameter value $T=6.610\,245\times10^{-3}$ and period doubling are related to the first two by the symmetry in the NE9 system. At $T=4.118\,200$ 0 at fold bifurcation occurs where the time-reversal symmetrically related orbits collide in a symmetric orbit and disappear. See

B. Tori and chaos for NE9

The presence of periodic solutions and tori was demonstrated for small values of a in Sec. III A. Interestingly destruction of tori can be observed when decreasing the parameter a. Decreasing from a = 0.1925 until a = 0.19026, we observe the changes of a double torus that is loosing smoothness, collapsing on itself and getting destroyed at some point; see Fig. 19. In Ref. 7, a chaotic set is identified for a = 0.55, x(0) = 0.5, y(0) = z(0) = 0, Kaplan–Yorke dimension $D_{KY} = 2.1544$. One can identify more chaotic sets, see

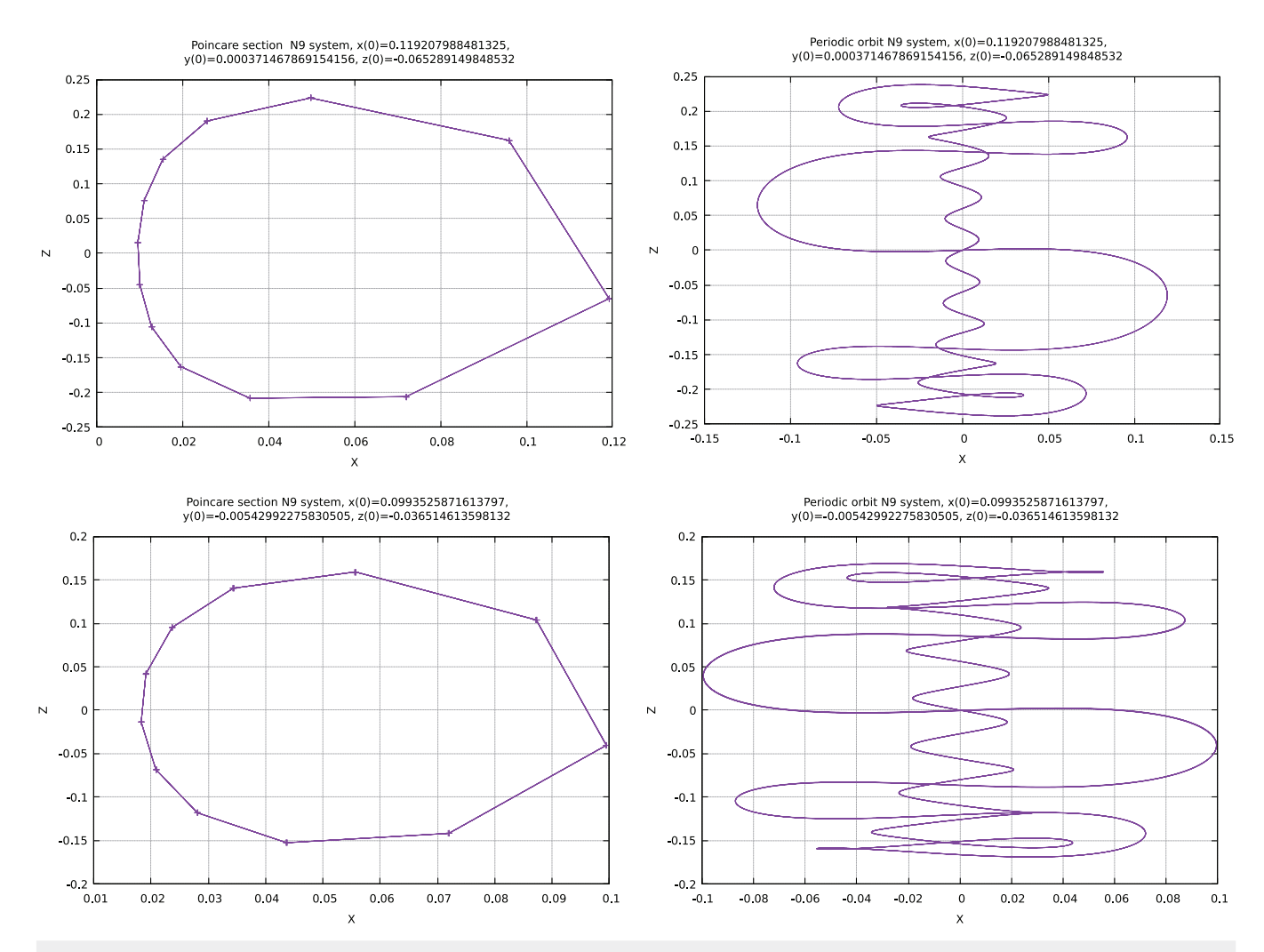


FIG. 12. We show a R-symmetric periodic stable solution of system NE9, a=0.01 (top position). Multipliers [0.999 999 995 10 044; 0.901 390 727 296 870 + 0.433 006 647 792 041i; 0.901 390 727 296 870 - 0.433 006 647 792 041i]. Left the Poincaré section and right the projection on the (x, z)-plane, period: 69.3070. Below an unstable solution, period 75.7092. Multipliers [0.999 999 999 630 394; 0.992 154 675 576 315 + 0.125 016 399 303 422i; 0.992 154 675 576 315 - 0.125 016 399 303 422i, located on the unit circle. Left the Poincaré section; right the projection on the (x, z)-plane.

Fig. 20 for the case $a = 0.206\,01$, the attractor is reminiscent of a full torus perforated an infinite number of times. It is important to understand its origin by analyzing the corresponding chaotic scenario. It turns out that by continuation of certain periodic solutions, a cascade of period doublings produces a chaotic attractor. This is the case when starting for instance with the periodic solution found by averaging, see the start of Subsection III A. The period doublings of periodic orbits P_i , $i = 1, \ldots, 5$ for several values of a are shown in Table V.

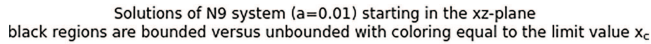
The ratio's $(a(P_{i+1}) - a(P_i))/(a(P_{i+2}) - a(P_{i+1}), i = 1, 2, 3$ are 5.464 63, 4.758 87, 4.663 11 and tend to the Feigenbaum constant $\delta = 4.6692$. In Fig. 21, we show the cascade of period doubling starting with a periodic R-asymmetric orbit.

Another way to display the chaotic attractor of Fig. 20 is showing it in three-space, see Fig. 22.

V. NUMERICAL COMPUTATION OF PERIODIC ORBITS

We describe the procedure that we followed to determine periodic solutions for the systems Sprott A and NE9. This is not straightforward as the solutions are embedded in families of tori and have to pass through slow manifolds.

Finding (unstable) periodic solutions in dynamical systems is important for understanding and clarifying the mechanisms behind the emergence of strange attractors and the ensuing chaos. A whole branch of mathematics called *Periodic Orbit Theory* is devoted to



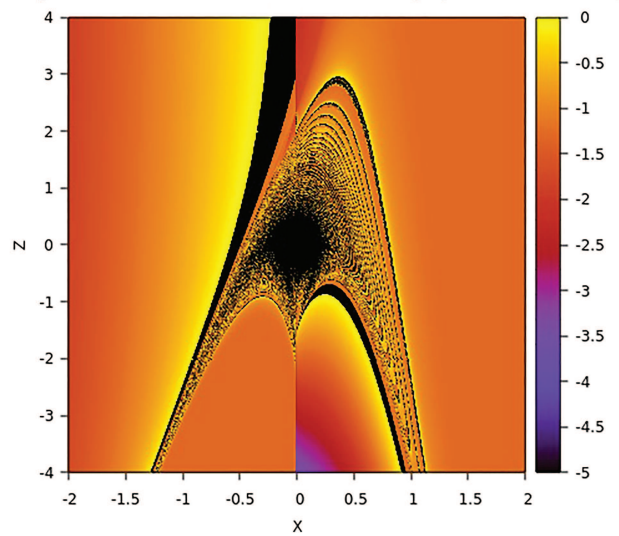


FIG. 13. The solutions of system NE9, a=0.01 that become unbounded start in the colored regions of the (x,z)-plane, the limiting value x_c is indicated by the color; the black regions correspond with bounded solutions. Left initial conditions starting at -2 < x < 2, -4 < z < 4; right a zooming in at the upper corner.

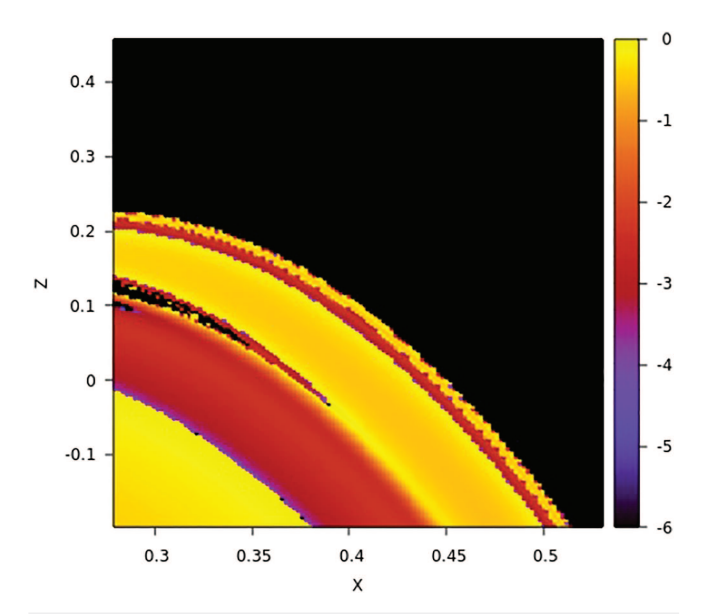


FIG. 14. The solutions of system NE9, a=0.55 that become unbounded start in the colored regions of the (x,z)-plane, the limiting value x_c is indicated by the color; the black regions correspond with bounded solutions.

this problem. There is a broad literature available in this area. See, for example, Ref. 4 and the literature therein. There is also a vast amount of literature and open source tools available on CAPD *Computer Assisted Proofs in Dynamics* and *interval arithmetics* to bridge the

gap between what is numerically observed in simulations and what can actually be proved theoretically.

In this paper, a combination of techniques has been used to locate periodic orbits. First, the time-reversal symmetry is exploited

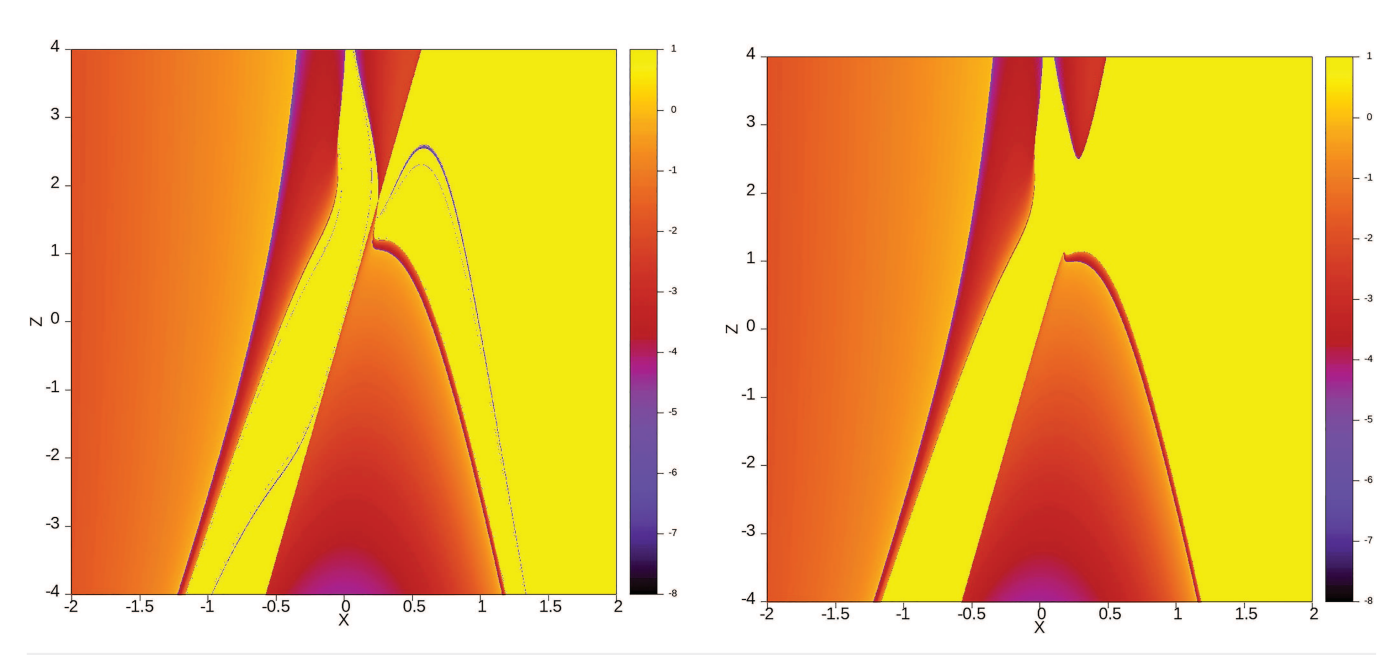


FIG. 15. Left the bounded solutions indicated by yellow regions in the x, z-plane of system NE9 with a=1; the solutions start at y(0)=-1/7. The manifold z=7x shows up, the nearby behavior looks complex. Right the case a=0.99, again starting at y(0)=-1/7.

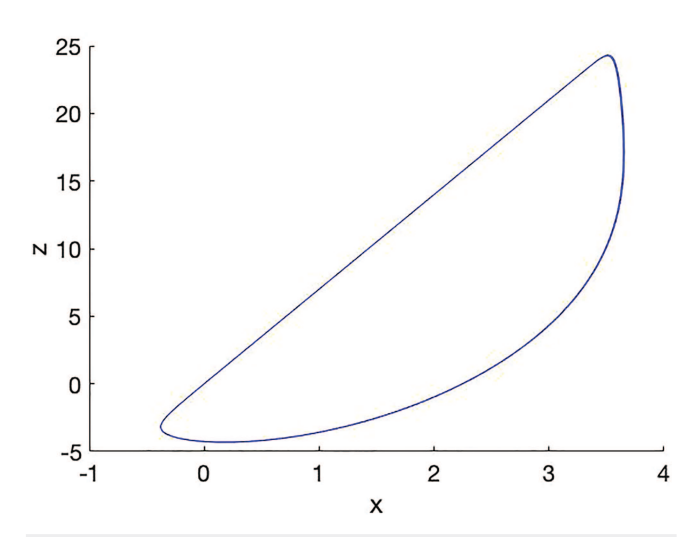


FIG. 16. Solutions in the x, z-plane of system NE9 with a=0.99; the solutions start at z(0)=7x(0), y(0)=-1/7 for x(0)=0.5,2,3, they can hardly be distinguished.

to find *R*-symmetric periodic solutions. Theorem 4.1 in Ref. 9 is heavily used to reduce the dimensionality of the space of initial conditions that yield *R*-symmetric periodic solutions from 3 to 1. For completeness, we reformulate here Theorem 4.1 as stated in Ref. 9 for flows.

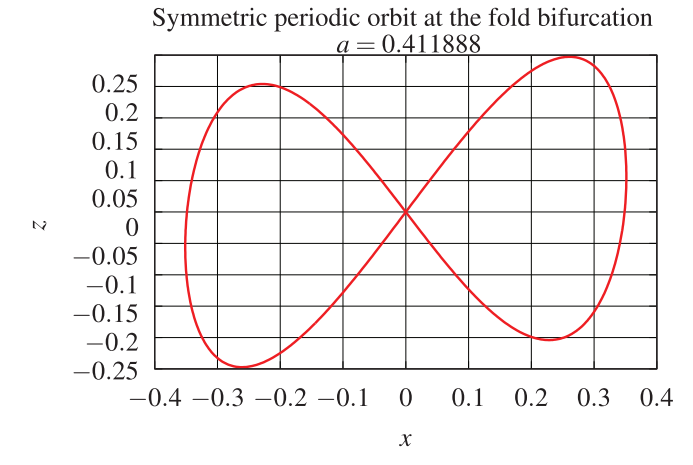


FIG. 18. Time-reversal symmetrically related orbits collide in a symmetric orbit and disappear.

Theorem V.1. Let o(x) be an orbit of the flow of an autonomous vector field with time-reversal symmetry R. Then,

- An orbit o(x) is symmetric with respect to R if and only if o(x) intersects Fix(R), in which case the orbit intersects Fix(R) in no more than two points and is fully contained in $Fix(R^2)$.
- An orbit o(x) intersects Fix(R) in precisely two points if and only if the orbit is periodic (and not a fixed point) and symmetric with respect to R.

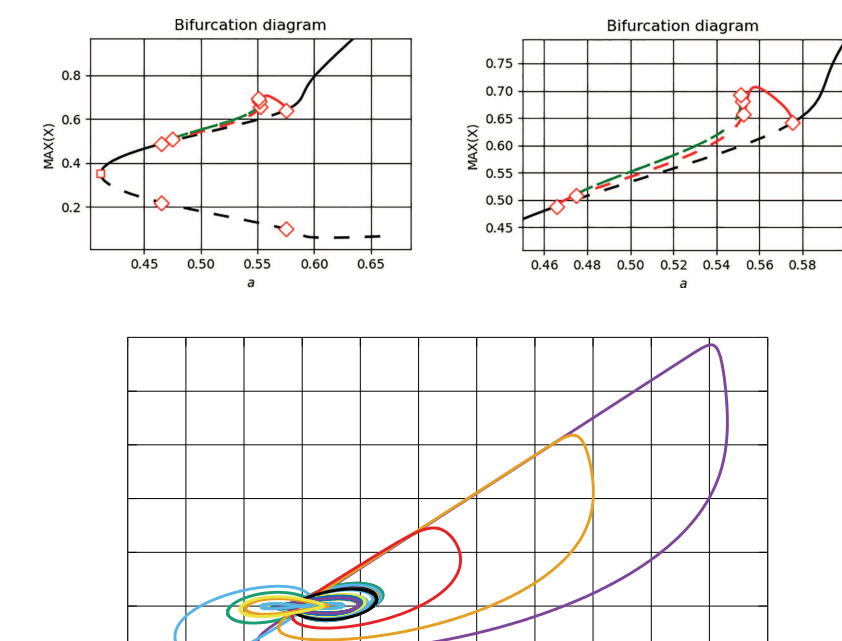
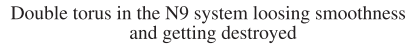


FIG. 17. Bifurcation diagram of the periodic orbit near the canard solution. The diamond symbol (upper figure) corresponds to period-doubling bifurcations. The square symbol indicates a fold bifurcation. Dashed lines mean the periodic orbit is unstable.



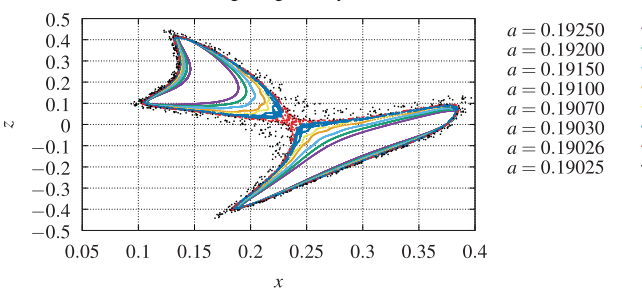


FIG. 19. Projection of a torus on the x, z-plane in system NE9, $a \approx 0.19$. Varying a, it gets into a state of non-smoothness and then becomes a double torus.

In the case of the Sprott A system, Fix(R) is the x axis. A direct consequence of the time-reversal symmetry is that R-symmetric periodic solutions of the Sprott A system are Lyapunov stable and have all multipliers on the unit circle. The Lyapunov stability of the R-symmetric periodic solutions makes numerical detection feasible. Using Theorem V.1, orbits starting on the x axis are numerically integrated and the number of intersections with Fix(R) is monitored. All orbits that approximately intersect Fix(R) twice are labeled as "potentially" periodic. This set of orbits is then used as first guess in continuation tools like Matcont⁵ and Auto⁶ to pinpoint their location exactly and compute their multipliers. Continuation even further with respect to the parameter a of the R-symmetric orbits as seeds yields branching point bifurcations with symmetry breaking yielding non-symmetric saddle periodic orbits. New unstable orbits are easily obtained from the R-symmetric ones through Branching Point Bifurcations. Most of the periodic orbits numerically found in this paper were obtained using this procedure. Note

TABLE V. Period doublings and corresponding values of a in system NE9.

Orbit	Value a	
P1	0.203 744 391	
P2	0.205 393 369	
Р3	0.205 695 124	
P4	0.205 758 533	
P5	0.205 772 131	

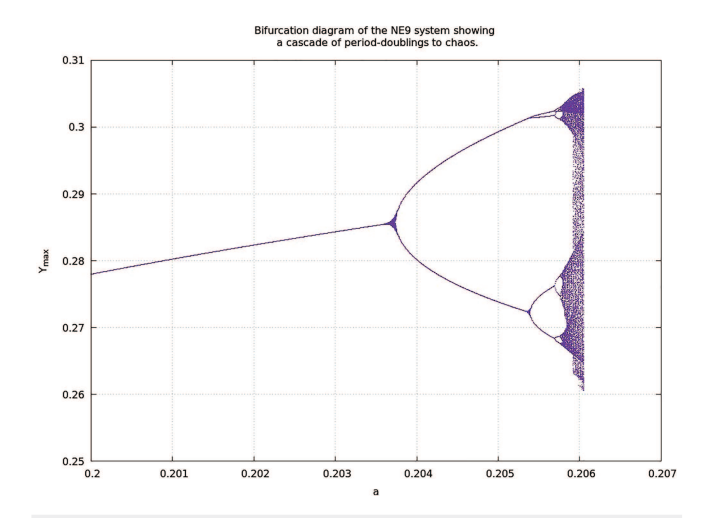
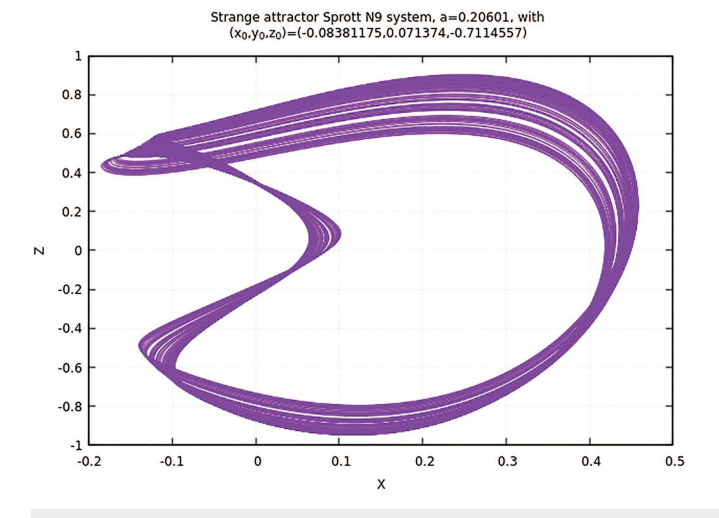


FIG. 21. The period-doubling cascade in system NE9 starting at a=0.2 leading to the chaotic set of Fig. 20 at $a=0.206\,01$.



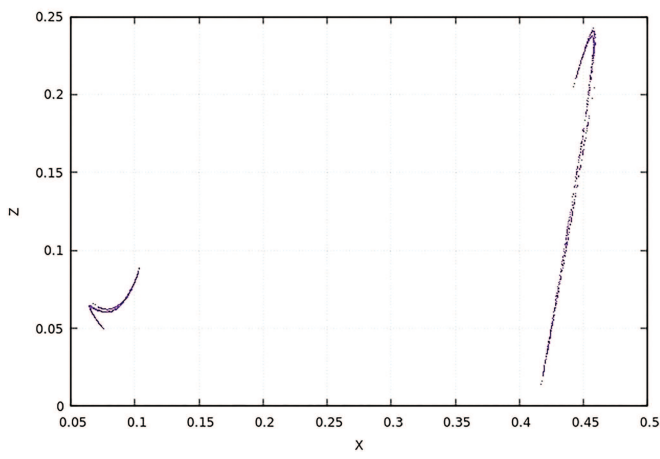


FIG. 20. Left the projection of a chaotic attractor on the x, z-plane in system NE9, a = 0.20601, initial values (x, y, z)(0) = -0.08311175, 0.071374, -0.7114557. Right the Poincaré section of the attractor transversing the plane y = 0.

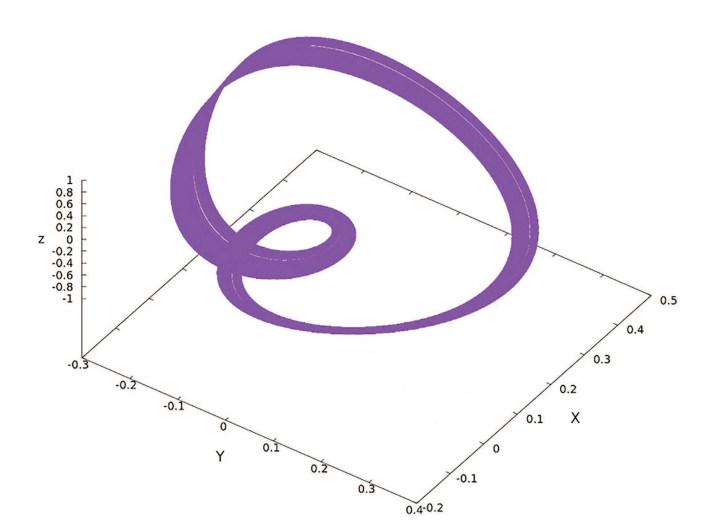


FIG. 22. Strange attractor from Fig. 20 at a = 0.20601 arising from a cascade of period doublings, here displayed in three-space.

that the procedure is not exhaustive, in the sense that it does not guarantee the finding of all periodic solutions in the Sprott A system. It is merely intended to be used as a "light weight" and easy to implement technique to quickly find stable and unstable periodic orbits and investigate their involvement, if any, in the observed complexity and chaos in the Sprott A and later on in the NE9 system. Not all unstable periodic solutions in the Sprott A system branched off from an R-symmetric periodic solution. A second approach to find these saddles numerically was implemented by using the result from Lemma I.4. The lemma guarantees a necessary condition for periodicity regardless of its stability character. The results of a numerical 3D sweep of initial conditions yields potential candidates for periodic solutions that are then used as first guess in Matcont to generate the precise location and the multipliers accurately.

VI. DISCUSSION AND CONCLUSIONS

- 1. As stated in Ref. 13, the presence of infinite families of tori for dissipative systems is a surprising phenomenon in systems Sprott A and NE9. It is analogous to the phenomenon of KAM tori near stable equilibrium of Hamiltonian systems. We have shown that for these dissipative systems, it arises from the time-reversal property of the systems.
- 2. Using rescaling of the differential equations, geometric singular perturbation theory adds valuable information on the qualitative and quantitative behavior of the solutions near the origin of phase-space and near infinity.
- 3. It would be interesting to study the remaining 14 systems listed in Ref. 7 for the presence of time-reversal, symmetry, and invariant manifolds. It was shown in Ref. 1 that for $0 < a \ll 1$ system NE8 contains a family with canard behavior, but after some time, the solutions tend to a stable periodic solution. System

- NE8 contains the z axis as an invariant manifold but misses out on the time-reversal with symmetry.
- 4. We found isolated tori and chaotic sets for the Sprott A and NE9 systems. It is an interesting open question how many more tori and chaotic sets exist in these systems.

ACKNOWLEDGMENTS

Earlier results in the literature were kindly communicated to us by M. Messias. Suggestions for editorial improvements by the referees are gratefully acknowledged.

AUTHOR DECLARATIONS

Conflict of Interest

The authors have no conflicts to disclose.

Author Contributions

Taoufik Bakri: Formal analysis (equal); Methodology (equal); Writing - original draft (equal). Ferdinand Verhulst: Formal analysis (equal); Methodology (equal); Writing – original draft (equal).

DATA AVAILABILITY

The data that support the findings of this study are available from the corresponding author upon reasonable request.

REFERENCES

- ¹C. Abdulwahed and F. Verhulst, "Recurrent canards producing relaxation oscillations," Chaos 31, 023121 (2021).
- ²V. I. Arnold, V. V. Kozlov, and A. I. Neishadt, Mathematical Aspects of Classical and Celestial Mechanics, Dynamical Systems III, edited by V. I. Arnlold (Springer,
- ³M.-C. Ciocci, A. Litvak-Hinenzon, and H. W. Broer, "Survey on dissipative KAM theory including quasi-periodic bifurcation theory," in Geometric Mechanics and Symmetry: The Peyresq Lectures, Lecture Notes 316 (Cambridge University Press, 2005), Vol. 306, pp. 303-355).
- ⁴J. Crofts, "Efficient method for detection of periodic orbits in chaotic maps and flows," Ph.D. thesis (University of Leicester, 2007).
- ⁵ A. Dhooge, W. Govaerts, Y. Kuznetsov, W. Mestrom, A. Riet, and B. Sautois, MATCONT and CL MATCONT: Continuation toolboxes in MATLAB, 07 2022.
- ⁶E. Doedel, A. R. Champneys, T. F. Fairgrieve, Y. A. Kuznetsov, B. Sandstede, and X. J. Wang, AUTO97: Continuation and Bifurcation Software for Ordinary Differential Equations (with HomCont) (Concordia University, Montreal, 1997), Silver ed., User's Guide.
- ⁷S. Jafari, J. C. Sprott, and S. Golpayegani, "Elementary quadratic chaotic flows with no equilibria," Phys. Lett. A 377, 699-702 (2013).
- ⁸M. Krupa and P. Szmolyan, "Extending geometric singular perturbation theory to nonhyperbolic points-Fold and canard points in two dimensions," SIAM J Math. Anal. 33, 286-314 (2001).
- ⁹J. S. W. Lamb and J. A. G. Roberts, "Time-reversal symmetry in dynamical systems: A survey," Physica D 112, 1 (1998).

 10 J. Laskar, "Frequency analysis of a dynamical system," Celestial Mech. Dyn.
- Astron. 56, 191–196 (1993).
- ¹¹P. De Maesschalck and S. Schecter, "The entry-exit function and singular perturbation theory," J. Differ. Equations 260, 6697–6715 (2016).

 12M. Messias and A. C. Reinol, "On the formation of hidden chaotic attractors
- and nested invariant tori in the Sprott a system," Nonlinear Dyn. 88, 807-821 (2017).

 $^{\rm 13}$ M. Messias and A. C. Reinol, "On the existence of periodic orbits and KAM tori in the Sprott a system: A special case of the Nosé-Hoover oscillator," Nonlinear

Dyn. 92, 1287–1297 (2018).

14J. A. G. Roberts and G. R. W. Quispel, "Chaos and time-reversal symmetry. Order and chaos in reversible dynamical systems," Phys. Rep. 216, 63-177 (1992).

15 J. C. Sprott, "Some simple chaotic flows," Phys. Rev. E **50**, R647–R650 (1994).

¹⁶A. N. Tikhonov, "Systems of differential equations containing a small parameter multiplying the derivative," Math. Sb. 31(73), 575-586 (1952)

(in Russian).

17F. Verhulst, Nonlinear Differential Equations and Dynamical Systems, 2nd ed.

(Springer, New York, 2000).

18 F. Verhulst, *Methods and Applications of Singular Perturbations* (Springer, New York, 2005).